Effects of fast ions on interchange modes in the Large Helical Device plasmas

Effects of fast ions on interchange modes in the Large Helical Device plasmas

Jonhathan PINON[1,2], Yasushi TODO[1,3], Hao WANG[1]

[1]National Institute for Fusion Science, National Institutes of Natural Sciences, Toki, Gifu 509-5292, Japan

[2]Phelma, Grenoble Institute of Technology, Grenoble, France

[3]Department of Fusion Science, SOKENDAI (The Graduate University for Advanced Studies), Toki, Gifu 509-5292, Japan

E-mail: todo@nifs.ac.jp

28 March 2018

Abstract.

Effects of fast ions on the magnetohydrodynamic (MHD) instabilities in a Large Helical Device (LHD) plasma with the central beta value (=pressure normalized by the magnetic pressure) 4% have been investigated with hybrid simulations for energetic particles interacting with an MHD fluid. When fast ions are neglected, it is found that the dominant instability is an ideal interchange mode with the dominant harmonic m/n=2/1, where m, n are respectively the poloidal and toroidal numbers. The spatial peak location of the m/n=2/1 harmonic is close to the $\iota = 1/2$ magnetic surface located at $r/a = 0.29$, where ι is the rotational transform and r/a is the normalized radius. The second unstable mode is a resistive interchange mode with m/n=3/2 that peaks at $r/a = 0.65$ nearby the $\iota = 2/3$ surface, which grows more slowly than the m/n=2/1 mode. The nonlinear coupling of the m/n=3/2 and 2/1 mode results in the growth of the m/n=5/3 mode and other modes leading to the global reduction and flattening of the pressure profile. When fast ions are considered with the central beta value 0.2% and the total pressure profile is kept the same, the ideal interchange mode with m/n=2/1 located close to the plasma center is stabilized while the resistive interchange mode with m/n=3/2 located far from the plasma center is less affected. The stabilization is attributed to the reduction of bulk pressure gradient, which is the dilution of the free energy source, because the energy transfer between the fast ions and the interchange modes is found to be negligible. For higher fast-ion pressure, Alfvén eigenmodes are destabilized by fast ions.

1. Introduction

The Large Helical Device (LHD) is a magnetical plasma confinement system with the heliotron configuration [1]. The major and minor radii are 3.9 m and 0.65 m, respectively. Pressure driven magnetohydrodynamic (MHD) instabilities such as the interchange instability and the ballooning instability are important for plasma stability in the LHD plasmas. For example, the flattening of electron temperature profile was observed with

m/n=2/1 magnetic perturbations around the $\iota = 1/2$ magnetic surface, where ι is the rotational transform [2]. The electron temperature profile flattening takes place when the plasma approaches the ideal stability boundary of m/n=2/1 mode. This indicates that the m/n=2/1 mode is an ideal interchange mode. MHD modes whose amplitude depends on the magnetic Reynolds number were also observed in the peripheral region. These modes can be identified as the resistive interchange modes. It was found for high-beta plasmas more than 3% that the maxima of the observed thermal pressure gradients at a low order rational magnetic surface in the peripheral region are relatively close to the marginal stability thresholds to the low-mode-number ideal MHD instability [3]. An interesting finding was that the pressure gradients including the beam pressure are well above the thresholds. This suggests that either the beam pressure does not contribute to the global ideal MHD instabilities or the beam pressure profiles are broader than the assumption for the analysis.

A theoretical analysis of high-beta MHD equilibria in the inward-shifted LHD configuration showed that the core plasma stays in the second stability, and the peripheral plasma stays near the marginally stable state against ballooning modes [4]. Nonlinear evolution of the MHD instabilities in LHD plasmas has been investigated with numerical simulations [5–9]. It was found that a large parallel thermal conductivity mitigates the ballooning instabilities and the associated pressure deformation [5,6]. The nonlinear MHD simulations clarified the physical mechanism of the core crush brought about by the resistive ballooning modes and their nonlinear coupling [9].

Recently, energetic ion driven resistive interchange mode (EIC) has been observed in the LHD experiments with the perpendicular neutral beam injection (NBI) [10]. The EIC is destabilized by fast ions generated by the NBI. The EIC was found to improve confinement of bulk plasma confinement at the cost of increasing fast-ion losses. In another study, hybrid simulations of energetic-particles interacting with an MHD fluid were performed based on the LHD experiment #47645 [11]. When the hybrid simulation was run continuously, the interchange mode grows more slowly than the Alfvén eigenmodes (AEs), but becomes dominant in the long time scale. The interchange mode oscillates with a constant frequency of 1 kHz. The interchange mode reduces the stored fast ion energy to a lower level than the AEs.

These studies motivated us to investigate the interactions between interchange modes and energetic particles in the LHD plasma #47645. The aim of this paper is to clarify the effects of fast ions on interchange modes. We have performed hybrid MHD simulations of interchange modes with and without fast ions. We first identify the MHD modes in the simulations without fast ions and then we study the interactions of fast ions with those modes via simulations for various initial fast ion pressures.

2. Method

We use the MEGA code [12–14], which solves the non-linear MHD equations coupled with equations describing the energetic particle dynamics. The MHD equations solved

by MEGA are

$$\frac{\partial \rho}{\partial t} = -\nabla \cdot (\rho \mathbf{v}) + \nu_n \triangle(\rho - \rho_{eq}), \tag{1}$$

$$\rho \frac{\partial}{\partial t}\mathbf{v} = -\rho \mathbf{v} \cdot \nabla \mathbf{v} - \nabla p + (\mathbf{j} - \mathbf{j}'_h) \times \mathbf{B} + \frac{4}{3}\nabla(\nu\rho\nabla \cdot \mathbf{v}) - \nabla \times (\nu\rho\boldsymbol{\omega}), \tag{2}$$

$$\frac{\partial p}{\partial t} = -\nabla \cdot (p\mathbf{v}) - (\gamma - 1)p\nabla \cdot \mathbf{v} + (\gamma - 1)\left[\nu\rho\omega^2 + \frac{4}{3}\nu\rho(\nabla \cdot \mathbf{v})^2 + \eta\mathbf{j} \cdot (\mathbf{j} - \mathbf{j}_{eq})\right] + \chi\triangle(p - p_{eq}), \tag{3}$$

$$\frac{\partial \mathbf{B}}{\partial t} = -\nabla \times \mathbf{E},\ \mathbf{j} = \frac{1}{\mu_0}\nabla \times \mathbf{B}, \tag{4}$$

$$\mathbf{E} = -\mathbf{v} \times \mathbf{B} + \eta(\mathbf{j} - \mathbf{j}_{eq}), \tag{5}$$

$$\boldsymbol{\omega} = \nabla \times \mathbf{v}, \tag{6}$$

where ρ, $\mathbf{v}$, p, and $\mathbf{B}$ are fluid density, fluid velocity, fluid pressure, and the magnetic field, respectively. The vacuum magnetic permeability is represented by μ_0, $\gamma = 5/3$ is the adiabatic constant, ν, ν_n and χ are artificial viscosity and diffusion coefficients chosen to maintain numerical stability. In this work, the dissipation coefficients ν, ν_n, χ, and η/μ_0 are assumed to be equal to each other. Unless otherwise specified, we use one value of the coefficients, 5×10^{-7} normalized by $v_A R_0$ where v_A is the Alfvén velocity at the plasma center, and R_0 is the major radius at the geometrical center of the simulation domain. The subscript "eq" represents the equilibrium variables. The Lundquist number is $S = av_A/(\eta/\mu_0) = 3 \times 10^5$, where a is the minor radius. In the LHD experiment #47645, the Lundquist number at the plasma center is about 200 times higher than that in our simulations. The time scales for restoring the equilibrium density and pressure profiles are a^2/ν_n and a^2/χ, respectively, which are equal to the resistive timescale $a^2/(\eta/\mu_0) = 40$ ms. These time scales are sufficiently longer than the time span of the simulations presented in this paper.

The MHD momentum equation [Eq. (2)] includes the energetic particle contribution in the energetic particle current density $\mathbf{j}'_h$ that consists of the contributions from parallel velocity, magnetic curvature and gradient drifts, and magnetization current. The $\mathbf{E} \times \mathbf{B}$ drift disappears in $\mathbf{j}'_h$ due to the quasi-neutrality [12]. The electromagnetic field is given by the standard MHD description. This model is accurate under the condition that the energetic particle density is much less than the bulk plasma density. The MHD equations are solved using a fourth order (in both space and time) finite difference scheme. The equations describing the energetic particles are the drift-kinetic equations using the guiding-center approximation. The energetic particles are simulated using the δf Particle-in-Cell (PIC) method. The equations of each particle are solved with a fourth-order Runge-Kutta method. The details of the equations can

be found in [13, 14]. In this study, finite Larmor radius effects are turned off.

The MEGA code participated in the code benchmark activity of the International Tokamak Physics Activity for a toroidal Alfvén eigenmode (TAE) in a tokamak plasma [15]. Good agreement was found for the frequency, growth rate, and spatial profile of the TAE among 9 codes including MEGA. The MEGA code has been applied to and validated on the energetic particle instabilities in LHD, JT-60U, and DIII-D plasmas [11, 16–20]. The MHD part of the MEGA code is called the MIPS code and well benchmarked for the ideal ballooning modes in an LHD plasma [21].

2.1. Equilibrium and fast ion pressure profile

The plasma that we investigate is based on the LHD experiment #47645 at $t = 0.58$s. The MHD equilibrium is constructed with the HINT code [22, 23]. The magnetic field at the plasma center is $B_0 = 0.62$T, and the major radius is $R_{\rm axis} = 3.75$m. The initial pressure profile and the rotational transform profile of the equilibrium magnetic field are shown in Fig. 1. Cylindrical coordinates (R, φ, z) are used for the HINT equilibrium and the simulations. The numbers of grid points are (128, 640, 128) for (R, φ, z) coordinates, respectively. For the purpose of the data analysis, Boozer coordinates [24] (r, ζ, ϑ) are constructed for the MHD equilibrium where r is the radial coordinate with $r = 0$ at the plasma center and $r = a$ at the plasma edge, and ζ and ϑ are the toroidal and poloidal angle, respectively. Both the bulk and the fast ions are hydrogen. The initial distribution function of fast ions is assumed for simplicity to be the slowing-down distribution with the maximum energy 180 keV and be isotropic in the velocity space, although the fast ions in the experiment are generated by the tangential neutral beam injection and are anisotropic in velocity space. The number of computational particles is 2.1×10^7.The fast ion pressure profile is assumed to be

$$p_{\rm EP} = \beta_{\rm EP} \frac{B_0^2}{2\mu_0} \exp\left[-\left(\frac{r}{0.4a} \right)^2 \right] . \tag{7}$$

For the simulation data analysis, all quantities (bulk density, MHD velocity, bulk pressure, magnetic field, fast ion pressure) are decomposed into Fourier series in the Boozer coordinate representation. For example, radial MHD velocity is decomposed to

$$v_r\left(\frac{r}{a}, \zeta, \vartheta, t\right) = \sum_{\rm m=0}^{\rm m=30} \sum_{\rm n=-10}^{\rm n=10} A_{\rm m,n}\left(\frac{r}{a}, t\right) \cos(\mathrm{m}\vartheta + \mathrm{n}\zeta) + B_{\rm m,n}\left(\frac{r}{a}, t\right) \sin(\mathrm{m}\vartheta + \mathrm{n}\zeta) \tag{8}$$

We will call r/a 'normalized radius'. Poloidal and toroidal mode numbers are represented by m and n, respectively. The mode numbers m and n should range from $0 \leq \mathrm{m} < +\infty$ and $-\infty < \mathrm{n} < +\infty$ but the restricted ranges $0 \leq \mathrm{m} \leq 30$ and $-10 \leq \mathrm{n} \leq 10$ are enough to analyze the simulation results effectively.

In the next sections, when we discuss harmonics, we refer to the harmonics of radial MHD velocity unless otherwise specified. 'Amplitude of the m/n=i/j harmonic' means

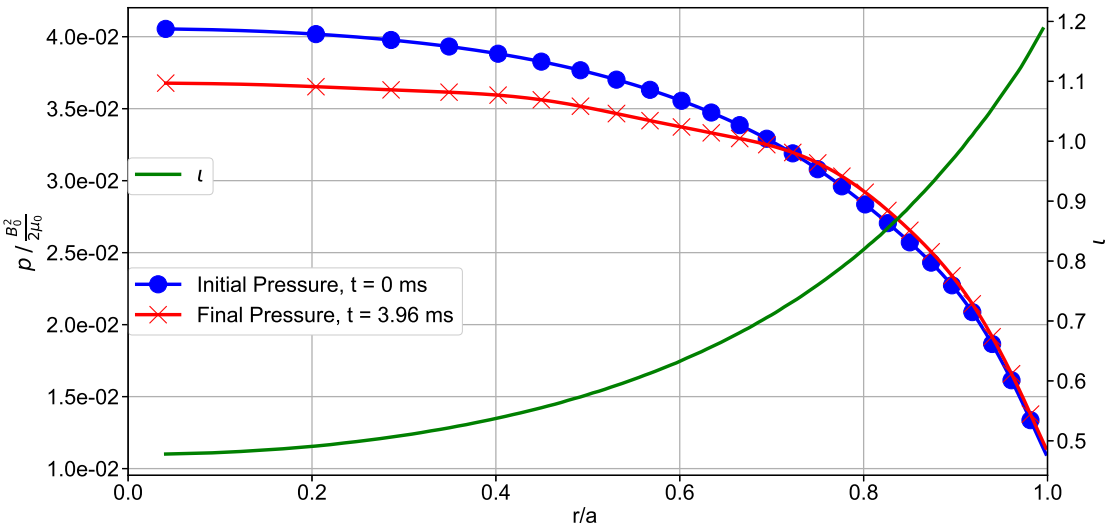

Figure 1. *Initial and final radial profile of bulk pressure in the simulation without fast ions (left axis). The rotational transform of the equilibrium magnetic field is also shown (right axis).*

$\sqrt{A_{i,j}^2\left(\frac{r}{a},t\right)+B_{i,j}^2\left(\frac{r}{a},t\right)}$. By 'variation', we mean the quantity at the instant t minus the quantity at the beginning of the simulation. For example, by 'pressure variation', we mean $p(t)-p(0)$.

3. Interchange modes without fast ions

3.1. Ideal interchange mode with m/n=2/1

We conducted a simulation without fast ions to investigate which types of MHD instabilities take place in the LHD plasma. Figure 1 shows the initial and final bulk pressure profiles and the rotational transform profile of the equilibrium magnetic field. We see that the final bulk pressure is reduced from the initial profile near the plasma center. The reduction of bulk pressure is brought about by MHD instabilities. We have found that the most unstable mode has the poloidal and toroidal mode numbers m/n=2/1. The radial profiles of the dominant harmonics for radial MHD velocity in the exponentially growing phase are shown in Fig. 2. The dominant harmonics are m/n=2/1, 0/9, 4/2, 1/1 and 3/1. The time evolutions of these harmonics at the peak locations are shown in Fig. 3. We fit the time evolutions with exponential curves, and find the growth rates. The growth rates are roughly the same $8.2-8.7\mathrm{ms}^{-1}$ for m/n=2/1, 0/9, 1/1 and 3/1 harmonics. This indicates that these harmonics constitute one eigenmode. Since the equilibrium magnetic field of the LHD plasma contains n=0, 10, 20, ... harmonics, n=1 and 9 harmonics can constitute together one eigenmode through the coupling with the n=10 equilibrium field component. On the other hand,

the m/n=4/2 harmonic grows with a growth rate twice that of the m/n=2/1 harmonic. This indicates that the m/n=4/2 harmonic is generated by the nonlinear coupling of the m/n=2/1 harmonic.

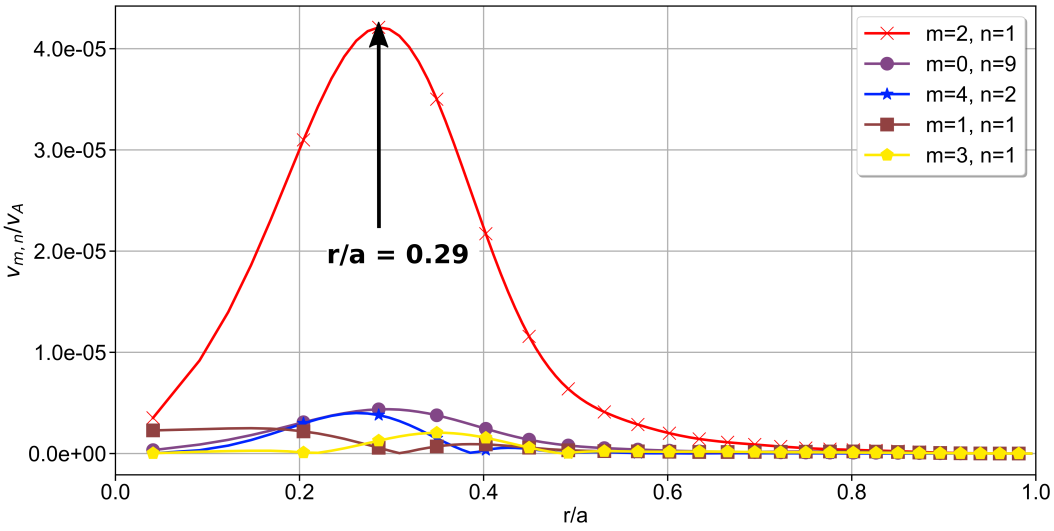

Figure 2. *Radial profiles of the 5 dominant radial MHD velocity harmonics at* $t = 1.35$ *ms in the simulation without fast ions.*

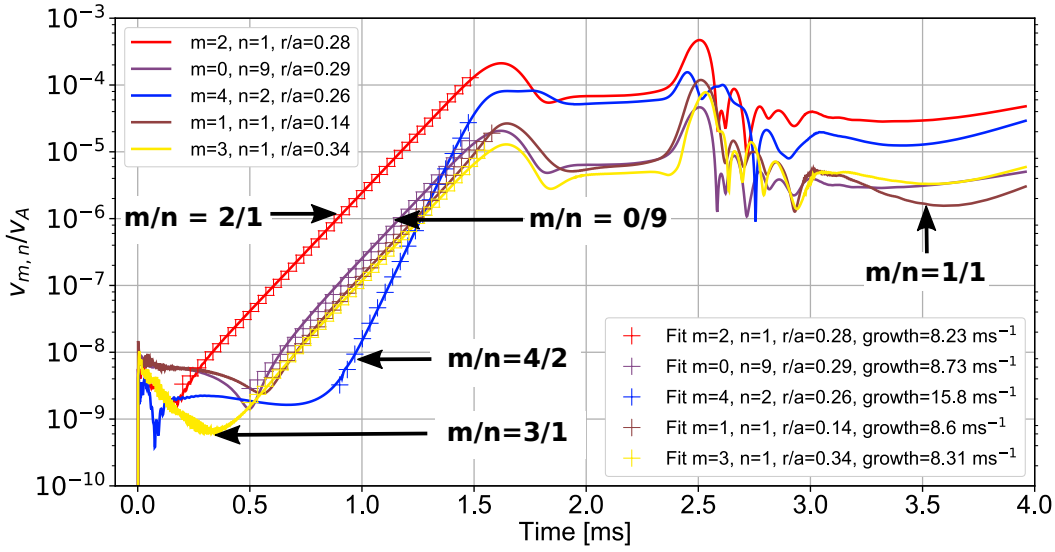

Figure 3. *Amplitude evolution of radial MHD velocity harmonics in the simulation without fat ions. The harmonics shown are the 5 dominant harmonics at* $t = 1.35$ *ms.*

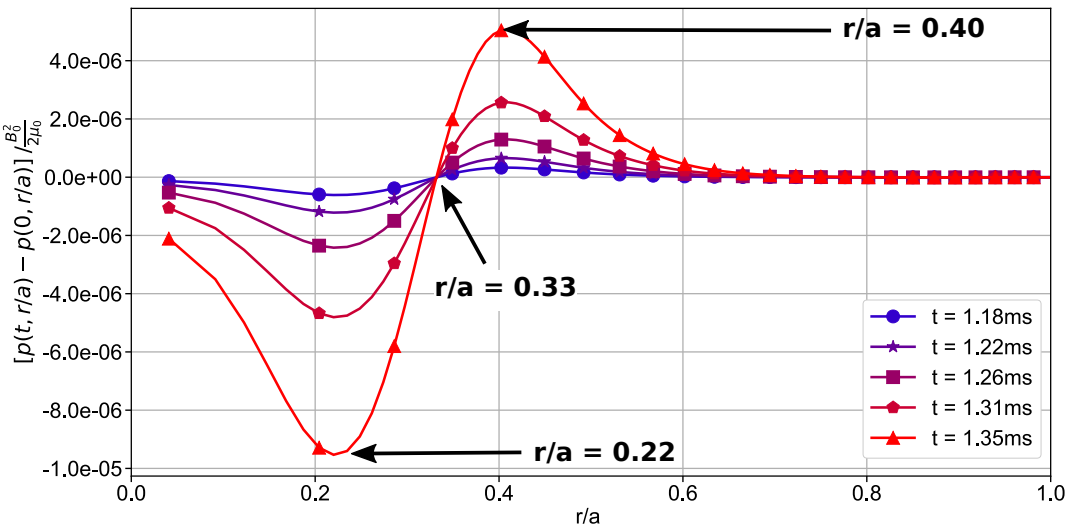

Figure 4. *Radial profiles of bulk pressure variation from* $t = 1.18$ *ms to* 1.35 *ms in the simulation without fast ions.*

The radial MHD velocity profile peaks at $r/a = 0.29$ where rotational transform is $\iota = 0.51$ as shown in Figs. 1 and 2. The spatial profile peak is located close to the rational surface with $\iota = 1/2$, and has one dominant harmonic m/n=2/1. This is a property of interchange mode. We also divide the bulk pressure evolution given by Eq. (3) into the following two groups,

$$\frac{\partial p_{\rm ideal}}{\partial t} = -\nabla\cdot(p\mathbf{v}) - (\gamma-1)p\nabla\cdot\mathbf{v}\ , \tag{9}$$

and

$$\frac{\partial p_{\rm dissipative}}{\partial t} = (\gamma-1)\left[\nu\rho\omega^2 + \frac{4}{3}\nu\rho(\nabla\cdot\mathbf{v})^2 + \eta\mathbf{j}\cdot(\mathbf{j}-\mathbf{j}_{eq})\right] + \chi\triangle(p-p_{eq})\ . \tag{10}$$

We integrate Eqs. (9) and (10) in time and space to investigate thermal energy evolution. We call thermal energy given by Eqs. (9) and (10) 'ideal thermal energy' and 'dissipative thermal energy', respectively in this paper. We confirmed that ideal thermal energy given by Eq. (9) decreases and is negative in the simulation without fast ions. This indicates that the instability is driven by bulk pressure. Furthermore, we confirmed that this mode is still unstable when all of the dissipation coefficients are set to be 0. Then, we conclude that the most unstable mode with the primary harmonic m/n=2/1 is an ideal interchange mode.

The radial profiles of bulk pressure variation during the exponentially growing phase are shown in Fig. 4. The pressure profile has one negative peak at r/a = 0.22 and one positive peak at r/a = 0.40. The two peaks grow exponentially with the same growth rate ($\sim$ 15 ms^{-1}), which is twice the growth rate of the m/n=2/1 interchange

mode. The pressure variation is almost zero where the mode amplitude is the highest ($r/a \sim 0.33$). This indicates that the pressure profile variation is brought about by the ideal interchange mode.

3.2. Resistive interchange mode with m/n=3/2

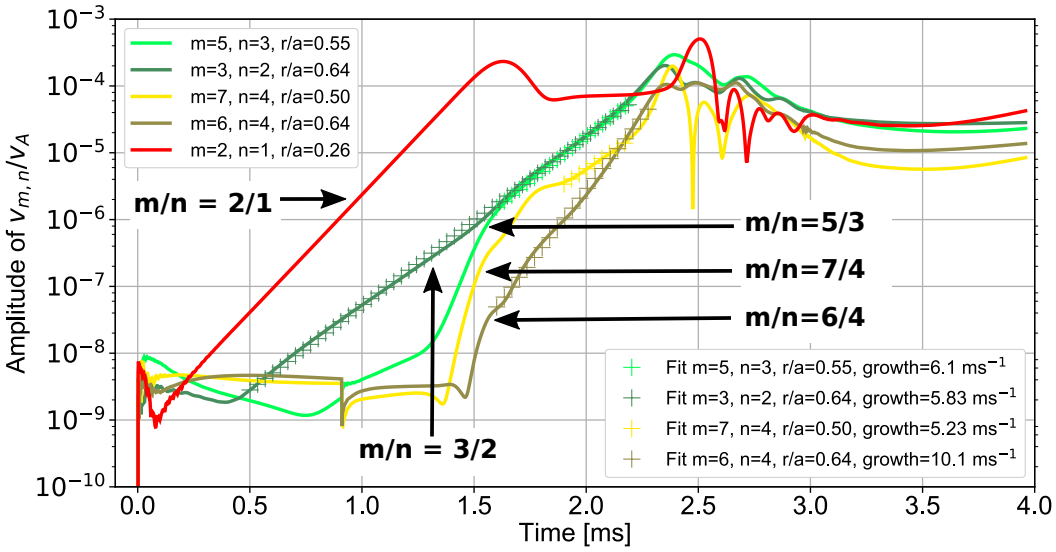

Figure 5. *Amplitude evolution of radial MHD velocity harmonics in the simulation without fast ions. The harmonics shown are the 5 dominant harmonics at t = 2.35 ms.*

After the saturation of the m/n=2/1 ideal interchange instability, another mode becomes dominant. Figure 5 shows the amplitude evolution of the top five harmonics whose amplitudes are the highest at t=2.35 ms. The spatial profiles of the top five harmonics are shown in Fig. 6. In addition to the m/n=2/1 harmonic of the ideal interchange mode, we find four new dominant harmonics, m/n=3/2, 5/3, 6/4, and 7/4. Besides the m/n=2/1 harmonic, only the m/n=3/2 harmonic grows exponentially shortly after the beginning of the simulation. This is a linear instability. The m/n=5/3 harmonic grows with the same rate as that of the m/n=3/2 harmonic after t = 1.6 ms. The m/n=5/3 harmonic can be generated by the nonlinear coupling of m/n=2/1 and 3/2 harmonics, and can grow with the same rate as that of the m/n=3/2 harmonic because the m/n=2/1 harmonic takes almost a constant amplitude at this time. The m/n=6/4 harmonic can be generated by the nonlinear coupling of m/n=3/2 harmonics in the MHD equations. This is supported by the fact that the growth rate of the m/n=6/4 harmonic (10.4 ms^{-1}) is roughly twice that of the m/n=3/2 harmonic (5.8 ms^{-1}). The time evolution of the m/n=7/4 harmonic is complicated. The m/n=7/4 harmonic may be generated by the nonlinear coupling of m/n=2/1 and 5/3 harmonics at $t \sim 2.0$ ms and generated by the nonlinear coupling of n=2 harmonics at $t \sim 2.2$ ms.

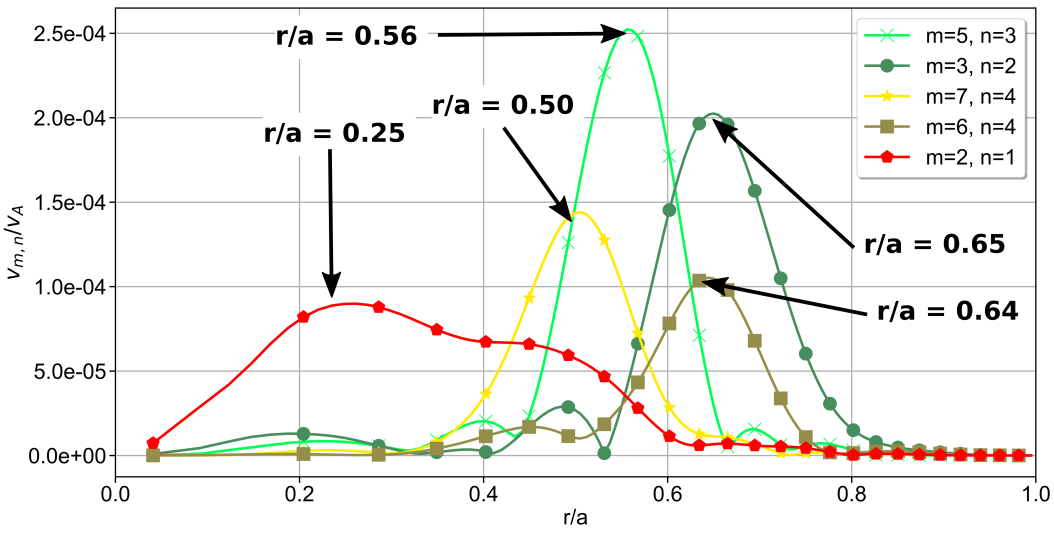

Figure 6. *Radial profiles of the 5 dominant radial MHD velocity harmonics at* $t = 2.35$ *ms in the simulation without fast ions.*

For the spatial profiles shown in Fig. 6, the spatial profile of the m/n=3/2 harmonic peaks at $r/a = 0.65$ where the rotational transform is $\iota = 0.67$, which is close to the rational surface with $\iota = 2/3$. The other harmonics with n=2 are much smaller than the m/n=3/2 harmonic, which can be confirmed with Fig. 6 where no n=2 harmonic other than m/n=3/2 is included for the top five harmonics. The linearly unstable mode with m/n=3/2 has only one dominant poloidal harmonic, which is a property of interchange mode. We performed an ideal simulation where all the dissipation coefficients were set to be 0, and found that the m/n=3/2 mode is stable. Then, we conclude that the instability with m/n=3/2 harmonic is a resistive interchange mode. In the ideal simulation, the nonlinearly generated harmonics m/n=5/3, 6/4, and 7/4 shown in Fig. 6 are negligible since the m/n=3/2 mode is stable.

We compare the pressure variation profiles from $t = 2.18$ ms to 2.35 ms in Fig. 7. The m/n=3/2, 5/3, 6/4, and 7/4 harmonics enhance pressure for $r/a > 0.65$ and reduce pressure for $r/a < 0.65$ leading to the flattening of pressure profile. The positive peak created by the ideal interchange mode with m/n=2/1 at $r/a \sim 0.4$, which is shown in Fig. 4, is reduced by the resistive interchange mode and the nonlinear modes to negative variation. This destabilizes again the m/n=2/1 mode at $t = 2.5$ ms and further flattens the pressure profile.

In this section, we investigated the MHD instabilities with the simulations without fast ions. We have found two linearly unstable modes, an ideal interchange mode with the primary harmonic m/n=2/1 and a resistive interchange mode with m/n=3/2. The spatial profiles peak at $r/a = 0.29$ and 0.65 for the ideal interchange mode and the resistive interchange mode, respectively. We will examine the impact of fast ions on

these instabilities in the next section.

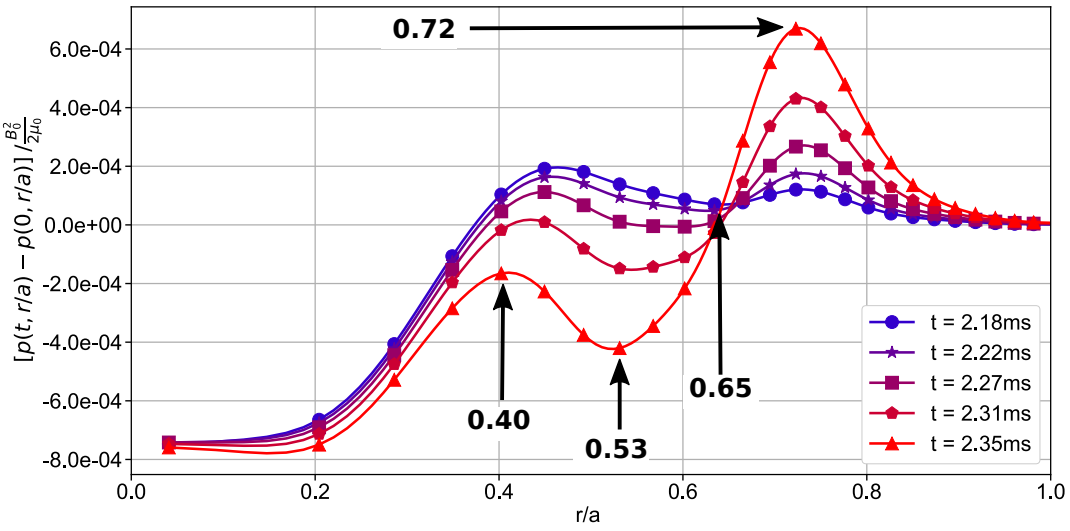

Figure 7. *Radial profiles of bulk pressure variation from $t = 2.18$ ms to 2.35 ms in the simulation without fast ions.*

4. Impact of fast ions on the interchange modes

4.1. Impact of β_{EP} on the instabilities

We performed 7 simulations where β_{EP} is 0.06%, 0.1%, 0.2%, 0.3%, 0.4, 0.5% and 1% to understand the effects of fast ions on the interchange modes. As total pressure, which is bulk pressure plus fast ion pressure, is fixed in our simulations, increasing β_{EP} means increasing fast ion pressure while decreasing bulk pressure. The impact of β_{EP} on bulk pressure and fast ion pressure is plotted in Fig.8. Bulk pressure decreases most at the center when β_{EP} increases because the fast ion pressure profile is a Gaussian profile in radius centered at $r/a = 0$ as given by Eq. (7).

We focus our study on the dominant harmonics of the ideal interchange mode and the resistive interchange mode, m/n=2/1 and 3/2. The amplitude evolutions of radial MHD velocity harmonic with m/n=2/1 at $r/a = 0.26$ are presented for various β_{EP} in Fig. 9. The growth rate and the maximum value of the amplitude decrease quickly with β_{EP}. When $\beta_{EP} = 0.1$ %, the growth rate reduces to 2.8 ms^{-1}. When $\beta_{EP} = 0.2\%$, the growth is no longer exponential, and it seems that the ideal interchange mode is stabilized.

For $\beta_{EP} = 0.3\%$, the mode grows again but this mode is actually a fast-ion driven mode. We see that the fast-ion driven modes can grow much more rapidly than the ideal interchange mode. The fast-ion driven modes oscillate with finite frequency. The properties of these fast-ion driven modes are very different from those of the ideal

interchange mode. The radial profiles of bulk pressure variation caused by these modes in the $\beta_{\rm EP} = 0.5\%$ simulation are shown in Fig. 10. Bulk pressure increases near the plasma center. The radial profiles of the 5 dominant radial MHD velocity harmonics are plotted in Fig. 11. The profile is slightly shifted inward from that of the ideal interchange mode shown in Fig. 2. The fast-ion driven mode is similar to the Alfvén eigenmode found in Ref. [11].

The amplitude evolution for the m/n=3/2 harmonic at $r/a = 0.68$ is shown in Fig. 12. The growth rate and the maximum value of the amplitude decrease slowly with $\beta_{\rm EP}$. However, contrary to the ideal interchange mode, the resistive interchange mode is unstable even for $\beta_{\rm EP} = 1\%$. At the high value of $\beta_{\rm EP}$ such as 0.5% and 1%, the rapid growth of the m/n=3/2 harmonic at the beginning of the simulation is caused by fast-ion driven modes and not by the resistive interchange mode.

Growth rates of the m/n=2/1 and m/n=3/2 harmonics with respect to $\beta_{\rm EP}$ are plotted in Fig. 13. The growth rates ($\gamma_{\rm growth}$) can be fitted by linear functions of $\beta_{\rm EP}$:

$$\gamma_{\rm growth} = a * \beta_{\rm EP} + b \tag{11}$$

The coefficients a and b for each mode are presented in Table 1. We see in Fig. 8 and Table 1 that increasing $\beta_{\rm EP}$ stabilizes the MHD modes while destabilizing fast-ion driven mode.

Mode	a [ms^{-1}/%]	b [ms^{-1}]
Ideal interchange mode	-54	8.1
Resistive interchange mode	-3.1	5.6
fast-ion driven modes	46	-9.0

Table 1. *Effects of $\beta_{\rm EP}$ on growth rate of the ideal and resistive interchange modes as well as on the fast-ion driven mode.*

4.2. Discussion

We have two hypotheses explaining the stabilization of the interchange modes by $\beta_{\rm EP}$. The first hypothesis is that fast ions interact with the interchange modes and absorb their energy, therefore stabilizing them. The second hypothesis is that the interchange modes are stabilized because bulk pressure decreases. Since both the ideal and resistive interchange modes are driven by bulk pressure, the reduction in bulk pressure leads to the stabilization of the interchange modes.

To see whether the first hypothesis is true, let us look at Figs. 14, 15, and 16 where the time evolutions of kinetic, magnetic, and thermal energies are shown for the $\beta_{\rm EP} = 0.1\%$, $\beta_{\rm EP} = 0.2\%$, and $\beta_{\rm EP} = 0.5\%$ simulations, respectively. For $\beta_{\rm EP} = 0.1\%$, the growth rates for both the ideal and the resistive interchange modes are reduced. However, we see in Fig. 14 that the energy transferred between the fast ions and the MHD fluid is almost zero. This indicates that fast ions neither stabilize nor destabilize

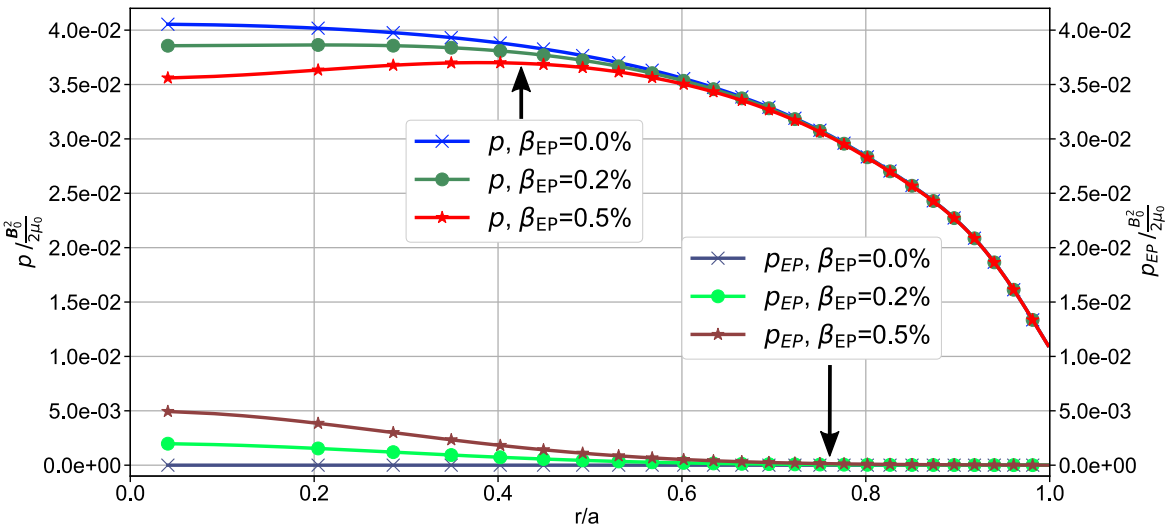

Figure 8. *Impact of β_{EP} on the initial bulk pressure profile (left axis) and on the initial fast-ion pressure profile (right axis).*

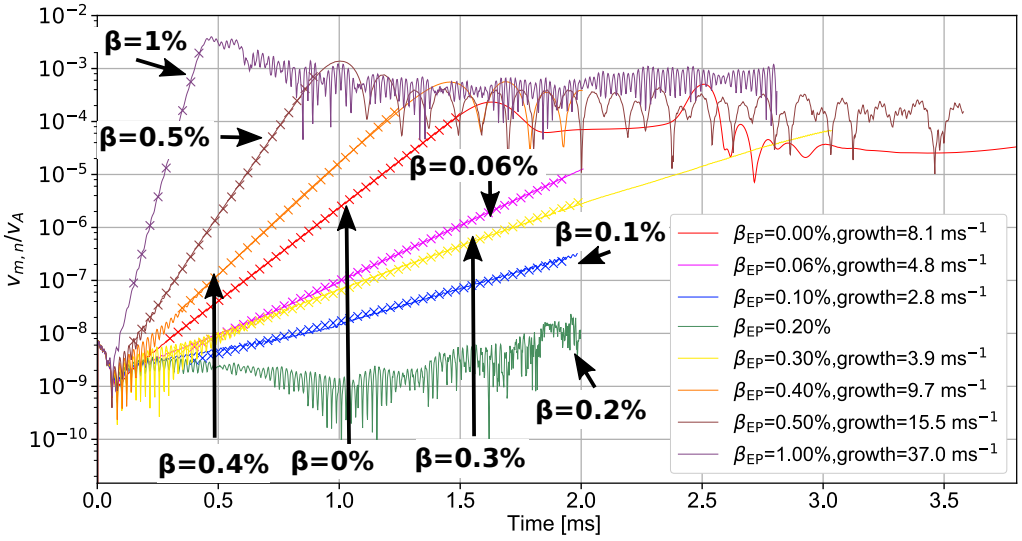

Figure 9. *Amplitude evolution of the radial MHD velocity m/n=2/1 harmonic for various β_{EP}.*

the interchange modes. For $\beta_{\mathrm{EP}} = 0.2\%$, where the ideal interchange mode is stabilized and the resistive interchange mode grows with a reduced rate, the energy transferred between the fast ions and the MHD fluid is still almost zero. This indicates that fast ions neither stabilize nor destabilize the resistive interchange. The first hypothesis is thus wrong. The interchange modes are stabilized because bulk pressure decreases when

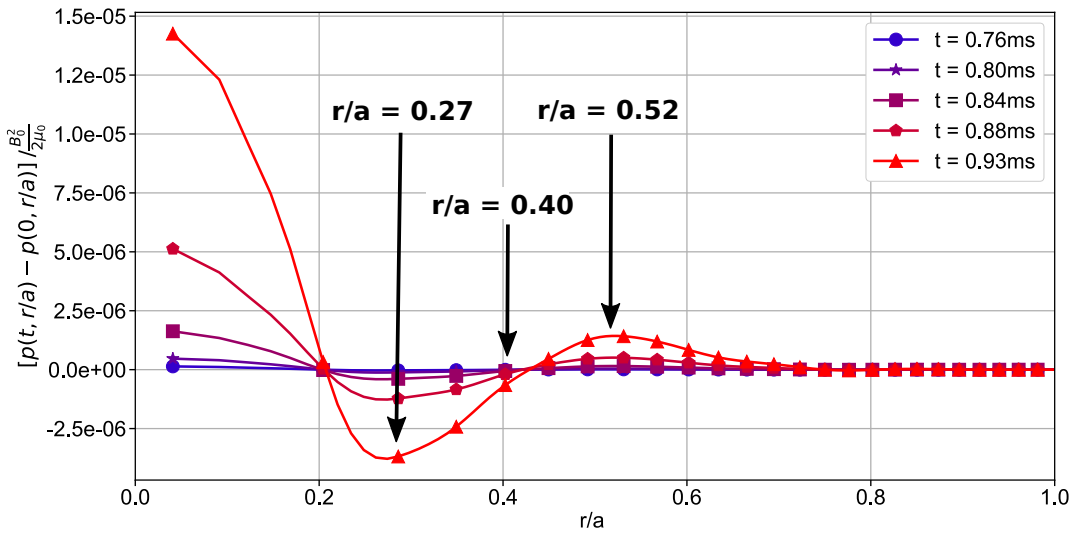

Figure 10. *Radial profiles of bulk pressure variation from* $t = 0.76$ *ms to* 0.93 *ms in the simulation with* $\beta_{\mathrm{EP}} = 0.5\%$.

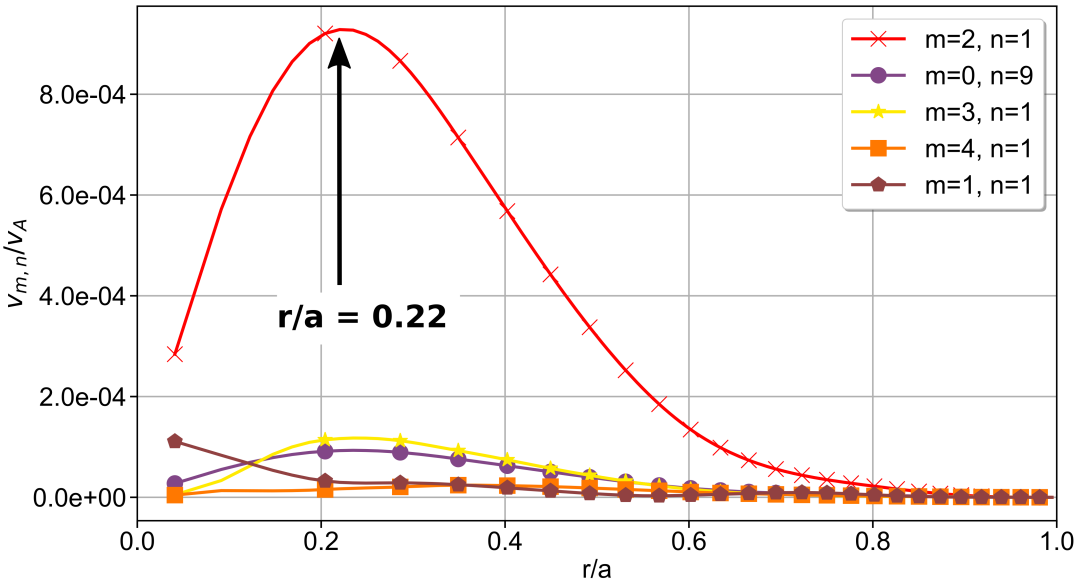

Figure 11. *Radial profiles of the 5 dominant radial MHD velocity harmonics at* $t = 0.93$ *ms in the simulation with* $\beta_{\mathrm{EP}} = 0.5\%$.

β_{EP} increases as shown in Fig. 8.

There is one major question why the ideal interchange mode is much more stabilized than the resistive interchange mode when β_{EP} increases? The answer lies in the radial location of the modes. In the case of the ideal interchange mode, the peak location

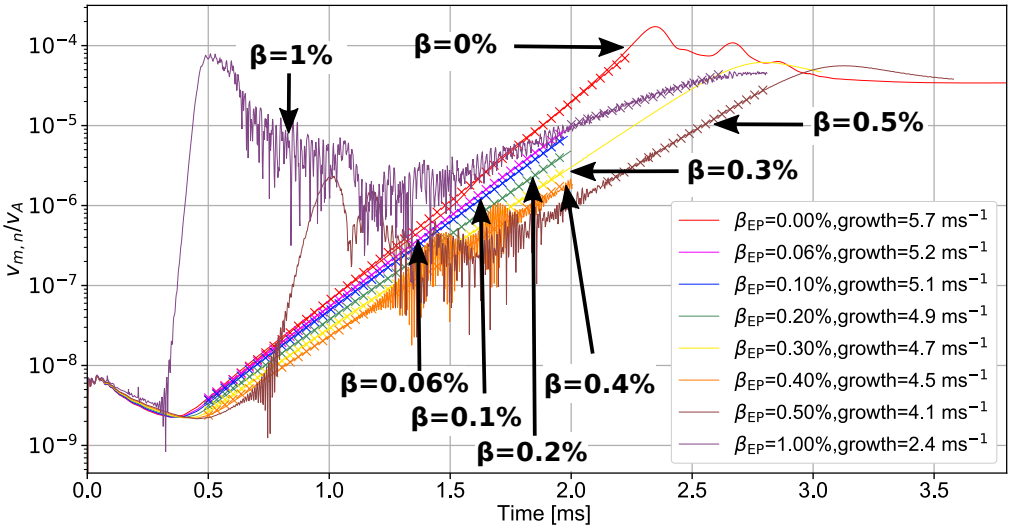

Figure 12. *Amplitude evolution of radial MHD velocity harmonic with m/n=3/2 for various* β_{EP}.

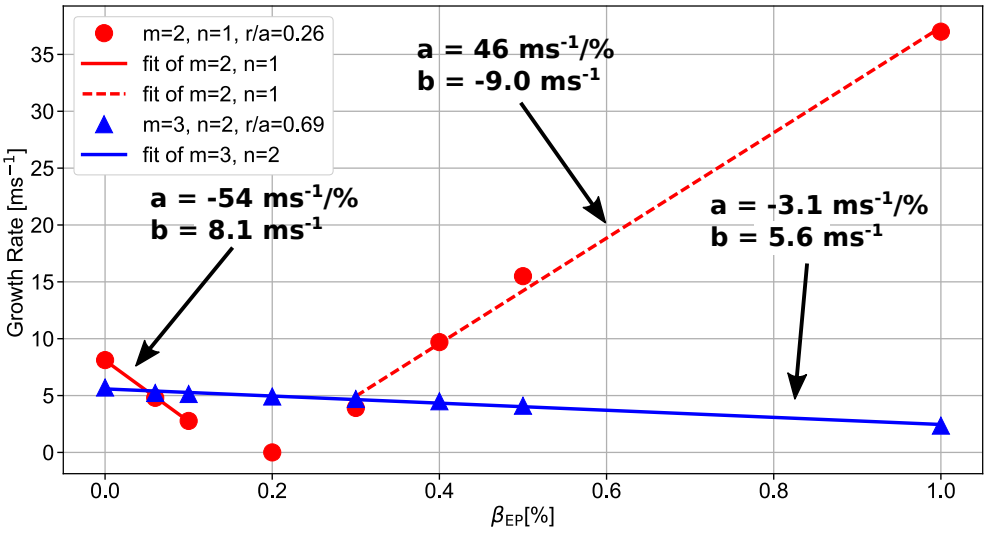

Figure 13. *Impact of* β_{EP} *on growth rate of the ideal interchange mode, the resistive interchange mode, and the fast-ion driven modes. The coefficients a and b refer to Eq. (11)*

is $r/a = 0.29$ whereas in the case of the resistive interchange mode, the peak location is $r/a = 0.56$. In addition, the decrease in bulk pressure with increasing β_{EP} is larger at the center than in the middle of the plasma (Fig. 8). It is therefore expected that the ideal interchange mode is much more affected than the resistive interchange mode.

This interpretation is supported by Fig. 17 that shows the growth rate of the m/n=2/1 modes versus the bulk pressure gradient at the $\iota = 1/2$ surface. Figure 17 demonstrates that the ideal interchange mode is stabilized for the weak or positive bulk pressure gradient with increasing β_{EP}. The centrally peaked fast ion pressure profiles that we assumed in this work is consistent with the fast ion pressure profiles simulated with the neutral beam injection and collisions that are shown in Fig. 7 in Ref. [11].

Lastly, let us notice that contrary to the interchange modes, EP-driven modes appear to heat bulk plasma. In Fig. 16, we see that both the ideal and dissipative energies are increasing while the energy transferred from the energetic particles to the bulk plasma is also increasing. This points out that the EP-driven modes heat the bulk plasma. Figure 11 shows that heating takes place at the central region of the plasma where the EP-driven mode is located. The heating occurs through the dissipative processes (viscous and resistive heating) and the ideal processes that are indicated by the increase in the ideal thermal energy shown in Fig. 16.

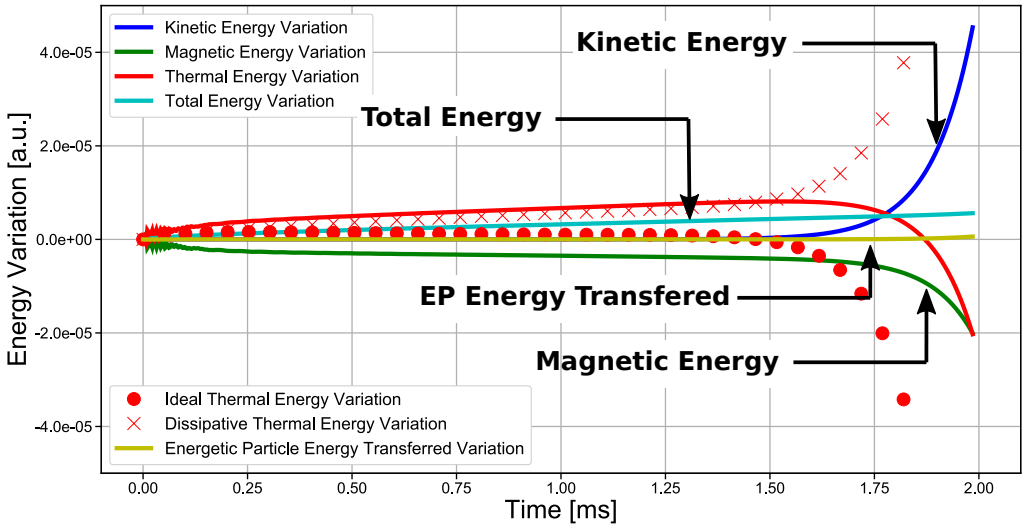

Figure 14. *Time evolutions of kinetic, thermal and magnetic energies in the $\beta_{\mathrm{EP}} = 0.1\%$ simulation. The energy transferred from the fluid to the energetic particles is also shown in yellow green.*

5. Conclusion

The goal of our study was to study the effects of fast ions on the interchange modes in the LHD. We accomplished the goal by simulating the plasma, for the LHD experiment #47645, with the MEGA code, and then analyzing the results.

Thanks to the analysis of the simulations without fast ions, we found that the dominant instabilities are an ideal interchange mode and a resistive interchange mode.

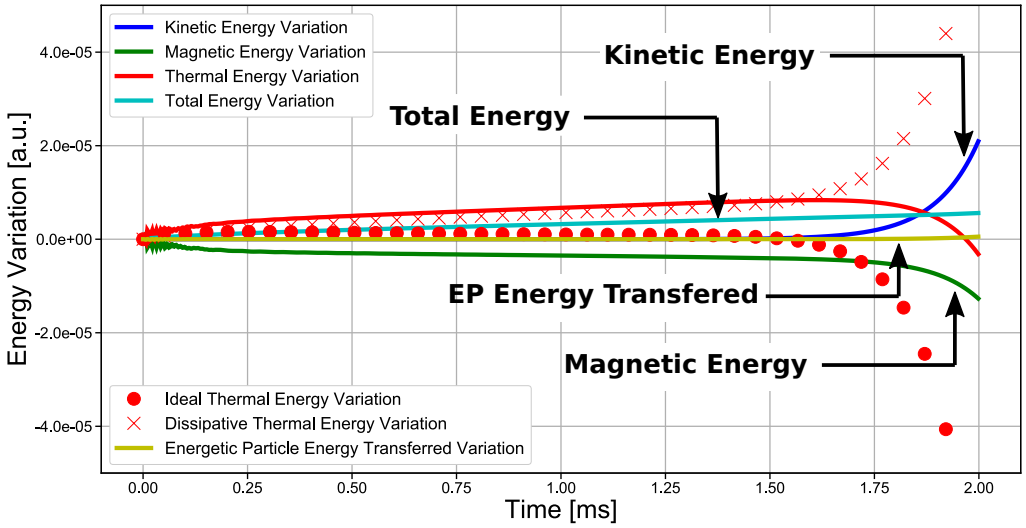

Figure 15. *Time evolutions of kinetic, thermal and magnetic energies in the* $\beta_{\mathrm{EP}} = 0.2\%$ *simulation. The energy transferred from the fluid to the energetic particles is also shown in yellow green.*

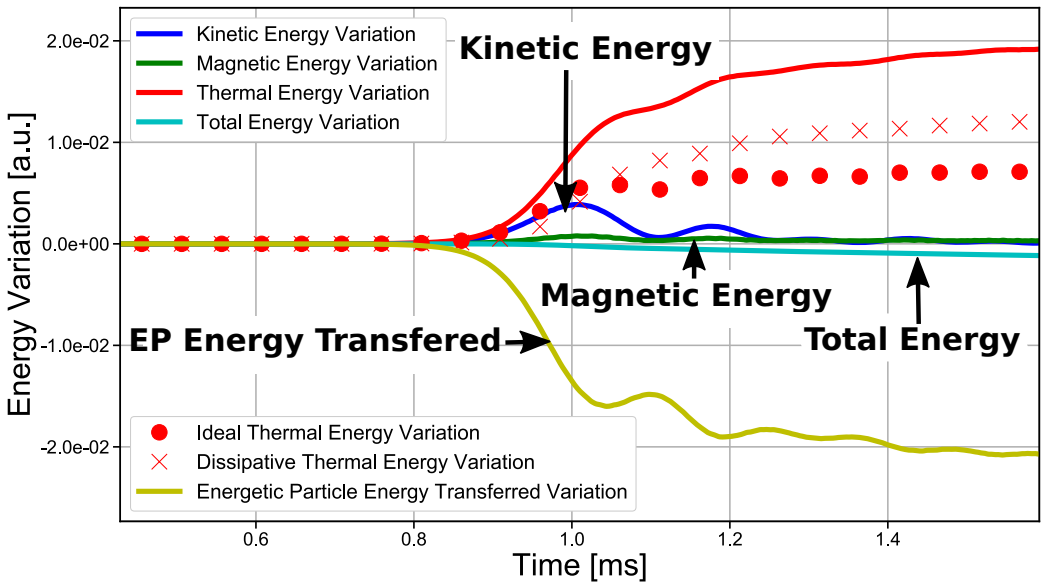

Figure 16. *Time evolutions of kinetic, thermal and magnetic energies in the* $\beta_{\mathrm{EP}} = 0.5\%$ *simulation. The energy transferred from the fluid to the energetic particles is also shown in yellow green.*

The dominant harmonic of the ideal interchange mode is the m/n=2/1 harmonic and the dominant harmonic of the resistive interchange mode is the m/n=3/2 harmonic.

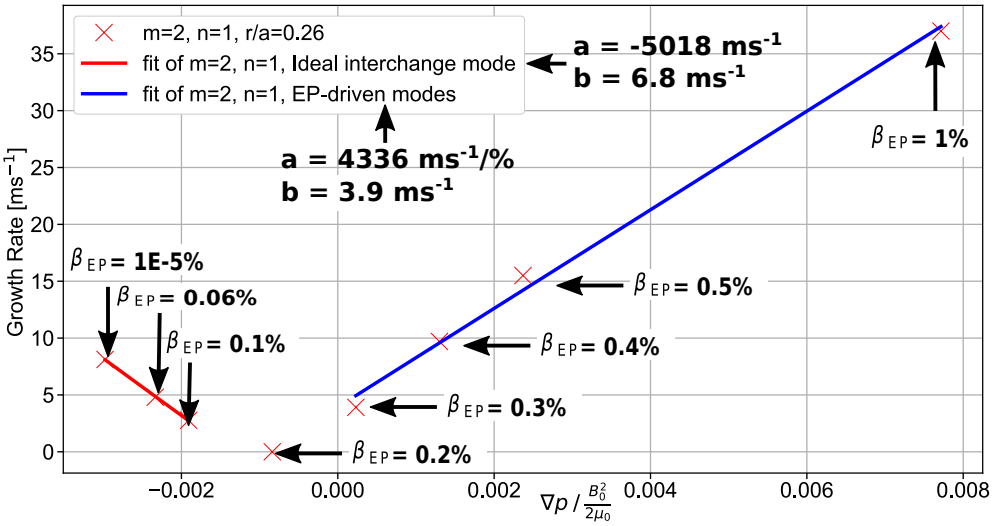

Figure 17. *Impact of the bulk pressure gradient at the $\iota = 1/2$ surface on the growth rate of the ideal interchange mode. The coefficients a and b refer to Eq. (11).*

The exponential growth rate of the ideal interchange mode is faster than that of the resistive interchange mode. The two linearly unstable modes and the other non-linearly generated modes resulted in the reduction of the central pressure profile by about 10% at the end of the simulation with dissipation.

Once the behavior of the plasma without fast ions was clarified, we studied the effects of fast ions on the interchange instabilities. When fast ions are considered with the central beta value 0.2%, the ideal interchange mode is stabilized while the resistive interchange mode located far from the plasma center is less affected. We found out that fast ions do not interact directly with the interchange modes. Then, the stabilization is attributed to the reduction of bulk pressure gradient, which is the dilution of the free energy source. We learned that fast-ion driven modes become dominant when fast-ion beta is higher than 0.2%. The growth rate of these modes can be several times higher than the growth rate of the interchange modes. The fast-ion driven modes transfer energy from the fast ions to the bulk plasma, which could be beneficial for nuclear fusion depending on fast-ion losses.

An interchange mode with frequency ∼1kHz that interacts with fast ions was found in Ref. [11]. We did not observe this interchange mode in the present paper. The difference between our work and Ref. [11] may arise from the fast ion velocity distribution. The isotropic velocity distribution is assumed in this work, while the fast ion velocity distribution formed with the neutral beam injection and collisions is anisotropic in Ref. [11]. For future works, it would be interesting to investigate the effects of the fast ion distributions with an anisotropic profile in velocity space and/or lower maximum energy close to the bulk temperature.

Acknowledgments

One of the authors of this paper, Jonhathan Pinon, a graduate student of Phelma, Grenoble Institute of Technology, would like to thank sincerely Phelma and his professors for teaching him sciences and for giving him the opportunity to carry research at the National Institute for Fusion Science as an internship student. He would especially like to thank Professor Elsa Merle Lucotte, Professor Jacob Lamblin, and Professor Olivier Meplan. He also wishes to thank the European organization FuseNet for the scholarship they graciously provided to him. Without this scholarship, doing the internship at NIFS would not have been possible. Numerical computations were performed at the Plasma Simulator of NIFS with the support and under auspices of the NIFS Collaboration Research program (NIFS17KNST110, NIFS16KNXN345). This work was partly supported by MEXT as "Priority Issue on Post-K computer" (Accelerated Development of Innovative Clean Energy Systems) and JSPS KAKENHI Grant Number 15K06652.

References

[1] A. Iiyoshi, A. Komori, A. Ejiri, M. Emoto, H. Funaba, M. Goto, K. Ida, H. Idei, S. Inagaki, S. Kado, O. Kaneko, K. Kawahata, T. Kobuchi, S. Kubo, R. Kumazawa, S. Masuzaki, T. Minami, J. Miyazawa, T. Morisaki, S. Morita, S. Murakami, S. Muto, T. Mutoh, Y. Nagayama, Y. Nakamura, H. Nakanishi, K. Narihara, K. Nishimura, N. Noda, S. Ohdachi, N. Ohyabu, Y. Oka, M. Osakabe, T. Ozaki, B.J. Peterson, A. Sagara, S. Sakakibara, R. Sakamoto, H. Sasao, M. Sasao, K. Sato, M. Sato, T. Seki, T. Shimozuma, M. Shoji, H. Suzuki, Y. Takeiri, K. Tanaka, K. Toi, T. Tokuzawa, K. Tsumori, K. Tsuzuki, K.Y. Watanabe, T. Watari, H. Yamada, I. Yamada, S. Yamaguchi, M. Yokoyama, R. Akiyama, H. Chikaraishi, K. Haba, S. Hamaguchi, M. Iima, S. Imagawa, N. Inoue, K. Iwamoto, S. Kitagawa, J. Kodaira, Y. Kubota, R. Maekawa, T. Mito, T. Nagasaka, A. Nishimura, C. Takahashi, K. Takahata, Y. Takita, H. Tamura, T. Tsuzuki, S. Yamada, K. Yamauchi, N. Yanagi, H. Yonezu, Y. Hamada, K. Matsuoka, K. Murai, K. Ohkubo, I. Ohtake, M. Okamoto, S. Satoh, T. Satow, S. Sudo, S. Tanahashi, K. Yamazaki, M. Fujiwara, and O. Motojima. Overview of the large helical device project. *Nuclear Fusion*, 39(9Y):1245, 1999.

[2] S. Sakakibara, K. Y. Watanabe, S. Ohdachi, Y. Narushima, K. Toi, K. Tanaka, K. Narihara, K. Ida, T. Tokuzawa, K. Kawahata, H. Yamada, A. Komori, and LHD Experiment Group. Study of mhd stability in lhd. *Fusion Science and Technology*, 58(1):176–185, 2010.

[3] K.Y. Watanabe, S. Sakakibara, Y. Narushima, H. Funaba, K. Narihara, K. Tanaka, T. Yamaguchi, K. Toi, S. Ohdachi, O. Kaneko, H. Yamada, Y. Suzuki, W.A. Cooper, S. Murakami, N. Nakajima, I. Yamada, K. Kawahata, T. Tokuzawa, A. Komori, and LHD experimental group. Effects of global mhd instability on operational high beta-regime in lhd. *Nuclear Fusion*, 45(11):1247, 2005.

[4] N. Nakajima, S. R. Hudson, and C. C. Hegna. Properties of ballooning modes in the planar axis heliotron configurations with a large shafranov shift. *Fusion Science and Technology*, 51(1):79–91, 2007.

[5] H. Miura, N. Nakajima, T. Hayashi, and M. Okamoto. Nonlinear evolution of magnetohydrodynamic instability in lhd. *Fusion Science and Technology*, 51(1):8–19, 2007.

[6] H. Miura and N. Nakajima. Influences of ballooning modes with moderate wave number on mhd equilibrium in lhd. *Nuclear Fusion*, 50(5):054006, 2010.

[7] N. Mizuguchi, Y. Suzuki, and N. Ohyabu. Nonlinear dynamics of a collapse phenomenon in heliotron plasma with large pressure gradient. *Nuclear Fusion*, 49(9):095023, 2009.

[8] K. Ichiguchi, Y. Suzuki, M. Sato, Y. Todo, T. Nicolas, S. Sakakibara, S. Ohdachi, Y. Narushima, and B.A. Carreras. Three-dimensional mhd analysis of heliotron plasma with rmp. *Nuclear Fusion*, 55(7):073023, 2015.

[9] M. Sato, N. Nakajima, K.Y. Watanabe, and Y. Todo. Characteristics of mhd instabilities for high beta plasmas in inward shifted lhd configurations. *Nuclear Fusion*, 57(12):126023, 2017.

[10] X. D. Du, K. Toi, M. Osakabe, S. Ohdachi, T. Ido, K. Tanaka, M. Yokoyama, M. Yoshinuma, K. Ogawa, K. Y. Watanabe, M. Isobe, K. Nagaoka, T. Ozaki, S. Sakakibara, R. Seki, A. Shimizu, Y. Suzuki, and H. Tsuchiya. Resistive interchange modes destabilized by helically trapped energetic ions in a helical plasma. *Phys. Rev. Lett.*, 114:155003, Apr 2015.

[11] Y.Todo, R.Seki, D.A. Spong, H.Wang, S.Yamamoto Y.Suzuki, N.Nakajima, and M. Osakabe. Comprehensive magnetohydrodynamic hybrid simulations of fast ion driven instabilities in a large helical device experiment. *Physics of Plasmas*, 24(8):081203, 2017.

[12] Y. Todo and T. Sato. Linear and nonlinear particle-magnetohydrodynamic simulations of the toroidal alfvén eigenmode. *Physics of Plasmas (1994-present)*, 5(5):1321–1327, 1998.

[13] Y. Todo, K. Shinohara, M. Takechi, and M. Ishikawa. Nonlocal energetic particle mode in a jt-60u plasma. *Physics of Plasmas*, 12(1):012503, 2005.

[14] Y. Todo. Properties of energetic-particle continuum modes destabilized by energetic ions with beam-like velocity distributions. *Physics of Plasmas*, 13(8):082503, 2006.

[15] A. Könies, S. Briguglio, N. Gorelenkov, T. Fehér, M. Isaev, P. Lauber, A. Mishchenko, D. A. Spong, Y. Todo, W. A. Cooper, R. Hatzky, R. Kleiber, M. Borchardt, G. Vlad, and ITPA EP TG. Benchmark of gyrokinetic, kinetic mhd and gyrofluid codes for the linear calculation of fast particle driven tae dyanamics. In *Proceedings of the 24th International Conference on Fusion Energy (San Diego, 2012) ITR/P1-34*. IAEA, 2012.

[16] H. Wang, Y. Todo, and Y. Suzuki. Simulations of energetic particle driven geodesic acoustic mode and global alfven eigenmode in 3-dimensional lhd equilibrium. In *Proceedings of the 26th IAEA Fusion Energy Conference (Kyoto, 2016) TH/P4-11*. IAEA, 2016.

[17] A. Bierwage, K. Shinohara, Y. Todo, N. Aiba, M. Ishikawa, G. Matsunaga, M. Takechi, and M. Yagi. Self-consistent long-time simulation of chirping and beating energetic particle modes in jt-60u plasmas. *Nuclear Fusion*, 57(1):016036, 2017.

[18] Y. Todo, M. A. Van Zeeland, A. Bierwage, and W.W. Heidbrink. Multi-phase simulation of fast ion profile flattening due to alfvén eigenmodes in a diii-d experiment. *Nuclear Fusion*, 54(10):104012, 2014.

[19] Y. Todo, M. A. Van Zeeland, A. Bierwage, W.W. Heidbrink, and M.E. Austin. Validation of comprehensive magnetohydrodynamic hybrid simulations for alfvén eigenmode induced energetic particle transport in diii-d plasmas. *Nuclear Fusion*, 55(7):073020, 2015.

[20] Y. Todo, M. A. Van Zeeland, and W.W. Heidbrink. Fast ion profile stiffness due to the resonance overlap of multiple alfvén eigenmodes. *Nuclear Fusion*, 56(11):112008, 2016.

[21] Y. Todo, N. Nakajima, M. Sato, and H. Miura. Simulation study of ballooning modes in the large helical device. *Plasma and Fusion Research*, 5:S2062, 2010.

[22] K. Harafuji, T. Hayashi, and T. Sato. Computational study of three-dimensional magnetohydrodynamic equilibriain toroidal helical systems. *Journal of Computational Physics*, 81:169, 1989.

[23] Y. Suzuki, N. Nakajima, K. Watanabe, Y. Nakamura, and T. Hayashi. Development and application of hint2 to helical system plasmas. *Nuclear Fusion*, 46(11):L19, 2006.

[24] Allen H. Boozer. Evaluation of the structure of ergodic fields. *Physics of Fluids*, 26(5):1288–1291, 1983.